Tool combination for the description of steel surface image and defect classification

Zoheir Mentouri[1], Hakim Doghmane[2], Kaddour Gherfi[1], Rachid Zaghdoudi[1], Hocine Bourouba[2],

[1] Research Center in Industrial Technologies – CRTI, P.O. Box 64, Cheraga, 16014 Algiers, Algeria
[2] Laboratory of Inverse Problems, Université 8 Mai 1945, BP 401, 24000 Guelma, Algeria

zoheirmentouri@yahoo.com, z.mentouri@crti.dz

Abstract. In industry, the automatic recognition of surface defects of flat steel products still represents a real challenge. Indeed, in addition to constraints such as the image noise or blur, there is neither an agreed standard of these defects nor a standard method that can ensure the defect identification, whatever are their size, shape, orientation and location. Thus, the complexity of the algorithm that deals with this matter always depends on specific needs of the application. In this paper, we give details on an approach that combines Gabor wavelets (GW) and the local phase quantization technique (LPQ), to describe the steel surface images, and uses the histogram to extract their characteristics. The defect classification is carried out by means of two classifiers, namely the nearest neighbors and the support vector machine. The method assessment is based on testing different parameter values of the used tools. The approach shows a good performance in terms of recognition rates and feature vector length, which impacts the computing time. Also, the study reveals its suitability for an online steel surface defect recognition application.

Keywords: Quality control, Computer vision, metal surface imaging, Filter bank application, pattern analysis and recognition.

1 Introduction

Vision based systems represent the contact-free, non-invasive and reliable solution that has found a large usage in many fields as biometrics, biomedical and aerial imaging as well as product inspection [1] In metal strip manufacturing plants, for instance, such a system assures the automated product quality monitoring. Since a good surface finish of the product is a necessity to meet all users' requirements, it has been, for a long time, online inspected by highly skilled operators. However, the increasing demand of steel goods has resulted in faster production lines and has made much more difficult the job of surface monitoring by human inspectors. Despite the introduction of machine vision based automatic inspection systems the issue of the detection and recognition of the steel surface flaws still present a challenging task.

Steel surface defects may be of different sizes, shapes, orientations and localizations within the image. Their random occurrence depends on the input product and the rolling process quality. For their detection and classification, numerous studies have been carried out, different approaches have been applied and significant results have been obtained, with regard to application needs [2, 3].

We can find methods that have used histogram properties and thresholding fast operations for the description of some defect types, which have been classified by SVM [4]; or other dynamic thresholding method of the pixel distribution, as in [5]. It helped to efficiently detect a complex rolled-in-scale defect in the hot rolling process. As for approaches in the spatial domain filtering, gradient operators, as a raw filtering means, have been used to define a seed point of a defective-region candidate in hot rolling steel process. It has been followed by a growing region operation to delimit a seam defect, and combined to thresholding and morphological operations to detect vertical scratches [6, 7]. Whereas Sobel, Gaussian, Wiener, Laplacian or other weighted averaging filters have been, according established procedures, although often complex, used for noise reduction, image deblurring, or for preserving defect edges. They have achieved interesting defect recognition rates [8]. Moreover, numerous statistical approaches have been used in re-encoding original image pixels to capture a maximum of the texture information of hot rolled steel images. For instance, with methods based on the LBP concept, as LTP, CLBP, AECLBP, ULBP and so on, or the methods based on the dual cross pattern DCP, the processed information has been gathered from just the image itself, i.e. the pixel neighborhood [9-14]. Whereas in BSIF method studies [15-18], the texture information has been revealed by the use of external filters, pre-learnt from natural images and applied either individually or in a multiscale approach.

Further, for more robustness against noise and image compression efficiency with a minimum loss of information, wavelet based approaches (Haar, Daubechies, Orthogonal) have been applied, mainly, for complex defect identification as scale on billets, plates and strips [19, 20]. Some other studies have showed an interest in the 2D Gabor transform. The filter complex responses have been thresholded or re-processed by a gradient based feature method to detect seam and scratch defects on plates and slabs [21, 22].

In this paper, we give a detailed scheme of building discriminant descriptors of defect images, based on the combination of Gabor wavelets (GW), known as efficient in image abrupt changes representation, and the Local Phase Quantization (LPQ) technique which captures the image local structure, while being invariant to the blur artifact. The merit of the proposed approach is of several folds: The mentioned tools, are for the first time combined and applied for steel flaws identification; a good performance is achieved in comparison with the tested methods or some previous works; the capability is proved in dealing with more than one surface flaw, unlike many other methods; and finally, with the used short feature vector, the suitability for a real time application is shown. In the remainder of this paper, an overview about the used techniques is given in section two, followed by the tool combination procedure. In the section four, the conducted experiment is exposed, the results are discussed and compared, and the computing time is assessed. The study ends with a conclusion.

2 Processing tools for defect image description

As reported in the literature, many techniques are used to extract features that best describe the defect image. Such methods have some advantages, but may present others weaknesses, as for instance some information loss. This, what may explain the fact that a defect image is often processed by more than one tool to provide a representative feature set, as discriminant as possible.

2.1 Gabor wavelets

Gabor transforms is known as a filtering operation, used to analyze the image texture by looking for specific frequency content in a specific direction and in a localized region around an image point. The Gabor wavelets represent complex band-limited filters, which are Gaussian kernel functions modulated by complex waves with a center frequency and orientation. The image representation by Gabor wavelet consists in convolving it with 2D Gabor kernels, defined by the expression in Equation 1 [23, 24]

$$\psi_{\mu,\nu}(z) = \frac{|k_{\mu,\nu}|^2}{\sigma^2} exp\left(-\frac{|k_{\mu,\nu}|^2 |z|^2}{2\sigma^2}\right)\left(exp\left(ik_{\mu,\nu}\right) - exp\left(-\frac{\sigma^2}{2}\right)\right) \quad (1)$$

Where |.| is a norm operator, μ and υ are respectively the orientation and the scale numbers of Gabor functions, $z=(x, y)$ is a vector with a spatial coordinates, σ is the standard deviation of the Gaussian function and $k_{\mu\nu}$ is the wave vector expressed by:

$$k_{\mu\nu} = k_{\nu}.exp(\, i\phi_{\mu}\,) \quad (2)$$

With: $kv=k_{max}/f_v$, $k_{max}=\pi/2$, $\Phi_\mu= \pi\mu/v$, $i = \sqrt{-1}$, and where f_v is the spacing factor between kernels in the frequency domain.
The number of the resulting kernel is determined by the product $\mu.v$. The Fig. 1 represents the imaged samples of Gabor wavelets real part.

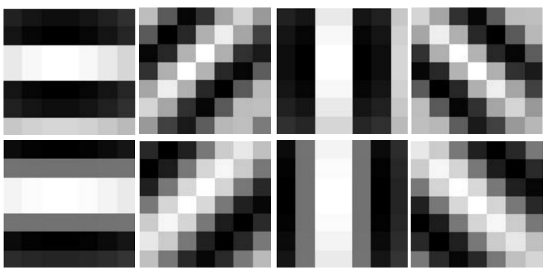

Fig. 1. Real part of Gabor filter bank of two scales, four orientations, and a medium window of 7x7 of size

2.2 Local phase quantization

Basically, the LPQ technique focuses on the extraction of the local phase information of an image, in the frequency domain [25, 26]. For this, it is assumed that an acquired/blurred image *b(x)* is a result of the 2D spatial convolution of an original image *i(x)* with *h(x)* a point spread function (PSF), showed in equation 3.

$$b(x) = i(x) * h(x) \tag{3}$$

This function is expressed, in the frequency domain, by the product of the Discrete Fourier Transform of the original image and the PSF, as in equation 4.

$$B(z) = I(z).H(z) \tag{4}$$

Where the phase of the resulting complex number is:

$$\angle B(z) = \angle I(z) + \angle H(z) \tag{5}$$

In LPQ, the PSF is considered centrally symmetric. Then, its phase, in the frequency domain takes the values as follows:

$$\measuredangle \mathrm{H(z)} = \begin{cases} 0 & if\ H(z) \geq 0 \\ \pi & if\ H(z) \prec 0 \end{cases} \tag{6}$$

Hence, at the frequencies where the *H(z)* is positive, its phase angle is of zero value, what means that the phase angle of *B(z),* in equation 5, does not change, and $\measuredangle I(z)$ reflects the blur invariant property. Thus, the local phase information of an input-image pixel is obtained by considering a neighborhood of *NxN* size and by computing the local spectra with the Short Term Fourier Transform:

$$I(z, x) = \sum_{m \in N^2} i(x - m).exp(-2\pi.z^T m) \tag{7}$$

Written in a vector form as:

$$I(z, x) = e_z^T i_x \tag{8}$$

Where *i(.)* is a square window from the image at each *x,* i_x is the vector of the pixel in the considered window and e_z is the 2-D DFT basis vector, at the frequency *z*.

The LPQ method focuses on only four frequency points, expressed by the following frequency vectors : $z_1[a, 0]^T$, $z_2[0, a]^T$,$z_3[a, a]^T$, $z_4[a, -a]^T$. Where *a* is a small scalar satisfying $H(z) \geq 0$, and for which, the complex elements of the resulting vector for each image pixel are:

$$I_x = [I(z_1, x), I(z_2, x), I(z_3, x), I(z_4, x)] \tag{9}$$

I_x is reorganized to have a new vector, constructed with the eight coefficients of both real and imaginary parts of the complex elements $I(z_i, x)$, as follows:

$$C_x = [Re\{I_X\}, Im\{I_x\}]^T = \{c_1(x), ..., c_8(x)\}^T \tag{10}$$

Finally, to encode the pixel phase information, the eight coefficients of C_x are binarized by applying the following scalar quantizer:

$$q_i = \begin{cases} 1 & if\ c_i(x) \geq 0 \\ 0 & if\ c_i(x) < 0 \end{cases} \quad (11)$$

Where $c_i(x)$ is the ith element in the C_x vector.

The new pixel code that represents the pixel local phase and reflects the blur invariant property, is computed by using the eight binary values q_i, as in equation 12.

$$lpq(x) = \sum_{1}^{8} q_i .2^{(i-1)} \quad (12)$$

3 Method combination scheme

As known, in pattern recognition, the objective of the feature extraction and classification tasks is, mainly the high rate achievement at an optimal computing time cost. However, in the considered application, this identification is more complex because the homogeneous steel surface structure can be affected not only by the occurring defect, but by the blur effect too. This may be induced by the moving state of the inspected surface or more generally by the industrial environment. Therefore, the image descriptor is built, by the proposed algorithm of Fig. 2, using together the two aforementioned tools to make it more discriminant.

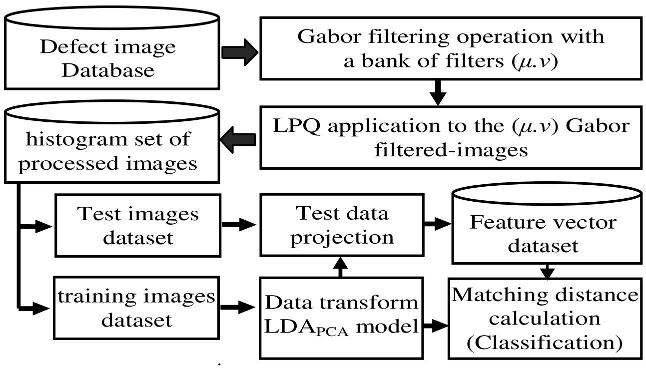

Fig. 2. General scheme of strip defect identification based on GW-LPQ process

The abrupt changes in the image defect are captured by Gabor wavelets which are proven to be efficient in characterizing the image properties and capturing the spatial frequency structure and orientations. Whereas, the local phase, which is relevant information in the defect image description, is extracted by the means of the local phase quantizer, known for its insensitivity to the image blur artifact.

4 Experiment and results

4.1 Used datasets

- **Northeastern University steel strip defect dataset**

In order to assess the proposed algorithm, the NEU Database [27], used in many published works, has served as a benchmark for a comparison. This dataset includes six defect types among the most frequent in a hot rolled strip: Rolled-in-scale (RS), Patches (Pa), Crazing (Cr), Pitted surface (PS), Inclusions (In) and Scratches (Sc). With enough within class variabilities and between class similarities, the defect classification is made more challenging. Some defect samples are depicted in Fig. 3.

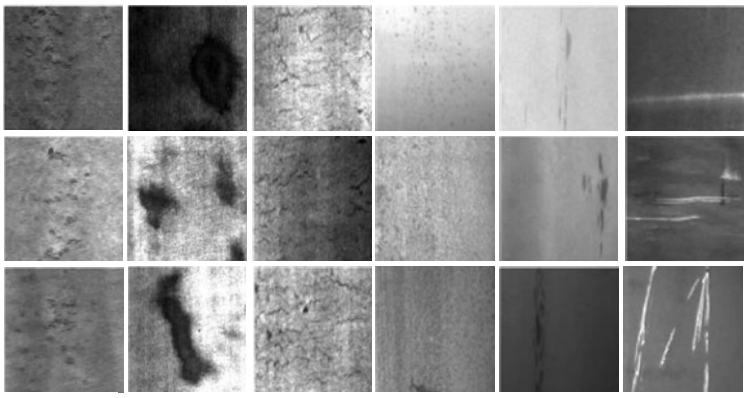

Fig. 3. Defect image samples from NEU Database

- **Research center defect dataset**

To better evaluate the proposed approach, we have used our defect dataset (RC_DDB). It includes the following six defect types that are the most frequent on the considered hot rolling line: Scale/under pickled (UP): Sticky scale or unwashed iron oxide covering a large surface, due to an improper descaling process; Fire-Crack (FC): Due to thermal shocks, some cracks generated on the finishing roll surface are transferred to the surface strip; Shell (Sh): non-metallic inclusions, initially on the slab sub-surface, appear as an overlapping material on the surface of the strip; Sticker (St): Distributed pits over the surface length of the strip and transferred by the dent marks of scrap stuck to the roll surface; Hole/massive rupture (MR): metal tears and perforations, caused by the poor ductility of the material or by a locally weakened section; Pinch roll marks (PM): Marks present at the head and tail ends of the hot band and caused by the abrasive and adhesive wear of the coiling-system pinch roll. Several variabilities in defect size, location, and orientation have been introduced in this dataset, to create more constraints in the defect detection of the 300 variant of each defect type. Some RC_DDB defect samples are depicted in Fig. 4.

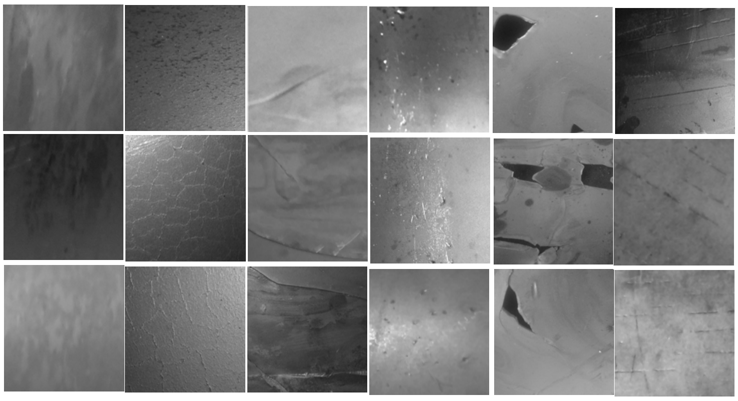

Fig. 4. Defect image samples from RC_DDB Database

4.2 Defect recognition procedure

Firstly, all database images are grouped in a global matrix in their vector form, prior to be processed. Gabor filters are constructed with one mother wavelet by dilation and many orientations/directions. Two sets of kernels are tested: $(\mu, \upsilon)=\{(4,2), (8,5)\}$. According to the general scheme in Fig. 2, the real part of Gabor wavelets (GW) is convolved with the defect images. Each of the $\mu x \upsilon$ resulting image is then processed by LPQ.

From each LPQ-output image a histogram is extracted and concatenated according to the first dimension, with the histogram of the previous LPQ-output. Thus, the final vector includes $\mu x \upsilon$ histograms, and represents a raw feature vector of a defect image.

As the process progresses, the raw feature vectors related to images of different classes, are concatenated columnwise, in a single and global matrix representing a new set of defect-image feature vectors.

A training partition is taken from this feature vector set and re-processed to reduce the dimension of the vectors, while keeping among their components, the most significant. This task is accomplished by combining PCA and LDA techniques, which have some known advantages. The first one can provide a good data representation of a same class, and the second has the property of discriminating the data of different classes. The obtained new reduced sub-space is used for the projection of the test image vectors, before their classification.

4.3 Results and discussion

Unlike others applications, as in biometrics, where the target in the image is enough sized and well shaped, a steel surface flaw may be spread and with no border as pitted surface, or may be scattered in small seeds of scale or inclusion, which may be confused with a noise. Hence, that importance in choosing the suitable processing tools. The NEU defect images are assumed to have been already sized and preprocessed as used in [27]. So, more filtering operation, or subsequent image decomposition in regions is unnecessary. Images are used as they are presented in the dataset. As for our RC_DDB, the raw defect images have been resized to 200x200 pixels, and processed by the widespread median filtering operation to eliminate outliers or extreme values.
For the two datasets, the defect recognition rate is computed several times, with the same method parameters. In each time, a different training set of the same size is randomly chosen; the average value of fifty trials is computed as well as the standard deviation. This latter is an indication about the result scatter or the confidence interval, depending on the training set composition [28]. So, it gives an overview about the effectiveness and robustness of the proposed approach. Tables 1 and 2 summarize the results obtained with the two assessed datasets.

Table 1. Average rates of NEU Database defect recognition.

Processing tools	Tool parameters	Feature vector	Classifier	Results (%)
GW_LDA$_{PCA}$	D=4, S=2	2048	KNN$_3$	82.40±1.37
			SVM$_{rbf}$	79.22±1.12
	D=8, S=5	10240	KNN$_3$	86.63±1.11
			SVM$_{rbf}$	88.36±1.01
LPQ_LDA$_{PCA}$	W.S.=9x9	256	KNN$_3$	96.18±0.57
			SVM$_{rbf}$	95.58±030
GW_LPQ	D=4, S=2, W.S.=9x9	2048	KNN$_3$	92.67±0.87
GW_LPQ_LDA$_{PCA}$	D=4, S=2, W.S.=9x9	2048	KNN$_3$	99.12±0.29
			SVM$_{rbf}$	98.67±0.32
	D=8, S=5, W.S.=9x9	10240	KNN$_3$	98.98±0.25
			SVM$_{rbf}$	98.44±0.86

As shown in the tables, the two processing tools GW and LPQ give moderate identification rates, when used individually. Increasing the direction and scale factors, in the Gabor method, improves the result; however, at the expense of the feature vector length, what highly impacts the processing time. Whereas the LPQ method performs better with a window size of 9x9 and a shorter feature vector.
As for the combination of GW and LPQ (GW_LPQ), it deals with all components of medium-length feature vectors, i.e. no data reduction. The obtained result is interesting, but in general, it does not improve any more that of the previous methods.

Table 2. Average rates of RC_DDB Database defect recognition.

Processing tools	Tool parameters	Feature vector	Classifier	Results (%)
GW_LDA$_{PCA}$	D=4, S=2	2048	KNN$_3$	76.73±1.80
			SVM$_{rbf}$	68.81±1.88
	D=8, S=5	10240	KNN$_3$	81.46±1.06
			SVM$_{rbf}$	78.80±1.21
LPQ_LDA$_{PCA}$	W.S.=9x9	256	KNN$_3$	78.81±1.15
			SVM$_{rbf}$	76.23±1.05
GW_LPQ	D=4, S=2, W.S.=9x9	2048	KNN$_3$	73.47±1.42
GW_LPQ_LDA$_{PCA}$	D=4, S=2, W.S.=9x9	2048	KNN$_3$	88.01±0.92
			SVM$_{rbf}$	86.07±1.08
	D=8, S=5, W.S.=9x9	10240	KNN$_3$	89.54±1.11
			SVM$_{rbf}$	88.25±1.46

The significant improvements are brought by the application of the LDA$_{PCA}$ technique, to the raw feature vectors, to have the new descriptor Gabor_LPQ_LDA$_{PCA}$. This performs much better than the other combinations, when used with the three "nearest-neighbors" classifier, and achieves the highest identification score. Whereas, lower performance is obtained and too much computing time is consumed by the same descriptor with a radial basis kernel function (Rbf) based SVM classifier.

The curves in the Fig. 5 express the recognition rates with different training set sizes.

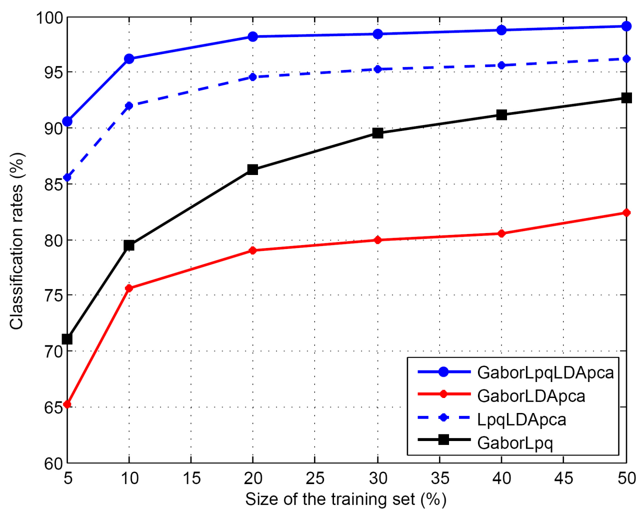

Fig. 5. Average rates of NEU Database defect recognition

It shows that with the proposed approach the result grows rapidly when the number of training images increases. Even with a training set selected from the whole used dataset (1800 images) and with a minimum size, more than 90% of the defects of the test images are correctly identified.

4.4 Previous works

The achievement of high rates in defect classification depends on many conditions. The performance of the used image acquisition equipment, the image quality and particularly the implemented software should help in overcoming the constraints related to the type and complexity of the considered defects. In this sub-section, we show (Table 3) the proposed approach outperforming some similar works that have used the same defect database, and the same size of the training set (50%).
A remark that is worth making, the rate of our algorithm is slightly lower than the one of the first line, in Table 3. This may be explained by the fact that this latter uses filters that are prelearnt from natural images bringing, thus, additional information. Whereas in our study, the information is gathered, exclusively, from the processed defect image. However, the result of our proposed approach is achieved with a much shorter feature vector. As shown, a raw feature vector of 2048 elements versus 4096 with the BSIF method.

Table 3. Recognition rates of NEU database Defects in some previous works.

Work Ref.	Features Descriptor	Classifier	Results (%)
A. Moussaoui [16]	BSIF_LDA	KNN	99.18±0.30
Kenchen S.[27]	SCN	SVM	98.60±0.59
M. W. Ashour [29]	DST–GLCM	SVM	94.11
Li Yi [30]	CNN	CNN	99.05
Kenchen S. [31]	AECLBP	SVM	98.93±0.63
Kenchen S. [31]	CLBP	SVM	98.28±0.51
Proposed algorithm	GW_LPQ_LDA	KNN	99.12±0.29

4.5 Processing time computation

The lasting time of the main tasks (feature extraction, data projection and classification) is computed to appreciate the approach suitability for an industrial application,. The results, in table 4, represent the average value of several trials of time computation related to all defect classes and to more than one defect by class.
This calculation is carried out on a machine endowed with an Intel i5-4590S CPU, 3.00 GHz, and 8 MB of dual channel memory, and a particular care has been paid to the code organization. As reviewed in the literature [2], the image processing time varies from 7 to 178 ms for process speed around 2 to 100 m/s. So we consider interesting, the time cost of our proposed approach, evaluated at 64,136ms/image. Obviously this time could be reduced with the use of specialized equipment.

Table 4. Average time per defect sample from NEU database.

Processing task	Time per Surface defect sample (ms)						Average time (T)
	Cr	In	PS	Pa	RS	SC	
Filtering operation	64,333	63,600	63,433	64,200	64,467	63,533	63,928
Projection	0,029	0,029	0,030	0,029	0,030	0,030	0,030
Classification	0,178	0,179	0,179	0,178	0,180	0,179	0,179
Total	64,541	63,808	63,642	64,407	64,677	63,742	64,136

5 Conclusion

The surface defect images of steel products are characterized by abrupt and random changes. They can also present other artifacts such as the blur. In this paper, we have proposed a new description of these images based on Gabor wavelets and the phase quantization technique. The approach has been evaluated using the NEU published dataset and our RC_DDB dataset. The two techniques have been applied successively to flaw images to capture changes in structures of different sizes and orientations and to use the non-blurred information. This made it possible to overcome constraints as inter-group similarities and intra-group differences of the different defect classes, and to perform consistently better than the other combinations. With the "nearest neighbors" classifier, the constructed discriminant defect image descriptors allow the achievement of the best classification rates with a much shorter feature vector compared to other methods. The obtained reduced standard deviation confirms the method robustness. Future works may focus on the application of other innovative methods and the recognition of the defects of other type of products, to provide suitable product quality-monitoring solutions.

References

1. J. Järvinen, J. Rauhamaa Real-time inspection of steel strip, -ABB Oy. https://pdfs.semanticscholar.org/f5a9/ aee3959f05492bc1106af5f2afd1c4d1d787.pdf
2. N. Neogi, D. K Mohanta, and P. K Dutta. Review of vision-based steel surface inspection systems. EURASIP Journal on Image and Video Processing (2014), http://jivp.eurasipjournals.com/content /2014/1/50.
3. Xiaohong Sun, Jinan Gu,, Shixi Tang and Jing Li Research Progress of Visual Inspection Technology of Steel Products-A Review. Applied Sciences 2018, 8, 2195; doi: 10.3390/app8112195, www.mdpi.com/journal/applsci.
4. DC Choi, YJ Jeon, SJ Lee, JP Yun and SW Kim Oilmarks Detection Algorithm in Steel Plates. Latest Trends on Systems,vol.I, 239–242, ISBN 978-1-61804-243-9.
5. D. Djukic, S. Spuzic Statistical Discriminator of Surface Defects on Hot Rolled Steel. Proceedings of Image and Vision Computing New Zealand 2007, 158–163, Hamilton, New Zealand, December 2007.

6. H Jia, YL Murphey, J Shi and T. Chang An Intelligent Real-time Vision System for Surface Defect Detection. IEEE-Proceedings of the 17th International Conference on Pattern Recognition, 2004, 2–5.
7. JP Yun, C Park, H Bae, H Hwang and S Choi Vertical Scratch Detection Algorithm for High-speed Scale-covered Steel BIC (Bar in Coil). International Conference on Control, Automation and Systems 2010, vol. 1 (KINTEX, Gyeonggi-do, Korea, 2010), 342–345.
8. Choi SH, Yun JP, Seo B, Park Y, KimSW(2007) Real-time defects detection algorithm for high-speed steel bar in coil, world academy of science. Eng Technol 25:66–70
9. Maenpaa T (2006) Surface Quality Assessment with advanced texture analysis techniques. Proc. of International Surface Inspection Summit, Luxembourg
10. Song K, Yan Y (2013) A noise robust method based on completed local binary patterns for hot-rolled steel strip surface defects. Appl Surf Sci 285P:858–864. Available at: https://doi.org/10.1016/j. apsusc.2013.09.002
11. Maoxiang CHU, Rongfen GONG (2015) Invariant feature extraction method based on smoothed local binary pattern for strip steel surface defect. ISIJ Int 55(9):1956–1962
12. Xiao M, Jiang M, Li G, Xie L, Yi L (2017) An evolutionary classifier for steel surface defects with small sample set EURASIP. J Image Video Process 2017:48. https://doi.org/10.1186/s13640017-0197-y
13. Zoheir Mentouri, Hakim Doghmane, Abdelkrim Moussaoui, Djalil Boudjehem. Surface flaw classification based on Dual Cross Pattern. 1st IEEE International Conference on Communications, Control Systems and Signal Processing. 16,17 March, 2020, El-Oued University, Algeria. DOI: 10.1109/CCSSP49278.2020.9151504
14. Mentouri, Z., Doghmane, H., Moussaoui, A. et al. Improved cross pattern approach for steel surface defect recognition. Int J Adv Manuf Technol 110, 30913100 (2020). https://doi.org/10.1007/s00170-020-06050-x
15. J. Kannala and E. Rahtu, Bsif: Binarized statistical image features. Proceedings of the 21st international conference on pattern recognition (ICPR 2012), Tsukuba, Japan, 1363-1366.
16. Z. Mentouri, A. Moussaoui, D. Boudjehem, H. Doghmane Steel Strip Surface Defect Identification Based on Binarized Statistical Features. Scientific Bulletin, Series B: Chemistry and Materials Science, Vol. 80 (4), 2018, ISSN 1454-2331, U.P.B Romania.
17. J. Ylioinas, J. Kannala, A. Hadid, M. Pietikainen, Face Recognition Using Smoothed High-Dimensional Representation, in Image Analysis, SCIA. Lecture Notes in Computer Science, vol 9127, ed. by R. Paulsen, K. Pedersen (Springer, Cham, 2015)
18. Mentouri, Z., Moussaoui, A., Boudjehem, D. et al. Steel Strip Surface Defect Identification using Multiresolution Binarized Image Features. J Fail. Anal. And Preven. (2020). https://doi.org/10.1007/s11668-020-01012-7
19. S. Ghorai, A. Mukherjee, M. Gangadaran, P.K. Dutta, Automatic Defect Detection on Hot-Rolled Flat Steel Products. IEEE Trans. Instrum. Meas. 62(3), 612–621 (2013)
20. W. Xiu-yong, X. Ke, X. Jin-wu, Application of Undecimated Wavelet Transform to Surface Defect Detection of Hot Rolled Steel Plates, in IEEE Congress on Image and, Signal Processing (2008), pp. 528–532
21. Choi DC, Jeon YJ, Yun JP, Yun SW, KimSW(2012) An algorithm for detecting seam cracks in steel plates. World Acad Sci Eng Technol Int J Mech Aerosp Ind Mechatron Manuf Eng 6(12): 2835–2838
22. Y.-J. Jeon, D.-C. Choi, J. P. Yun, C. Park, and S. W. Kim Detection of scratch defects on slab surface. Proceedings of the 11th International Conference on Control, Automation and Systems (ICCAS '11), (2011), 1274–1278, Gyeonggi-do, South Korea, October 2011.
23. Yu Cheng, Zhigang Jin, Hongcai Chen,Yanchun Zhang and Xiaoxia Yin A fast and robust face recognition approach combining Gabor learned dictionaries and collaborative representation. Int. J. Mach. Learn. & Cyber. (2016) 7:47–52, doi: 10.1007/s13042-015-0413-y. Springer-Verlag Berlin Heidelberg 2015.
24. Wang Xuan, Lei Li and Wang Mingzhe Palmprint verification based on 2D – Gabor wavelet and pulse-coupled neural network. Knowledge-based system 27 (2012),451-455, doi:10.1016/j.knosys.2011.10.008. Journal homepage: www.elsevier.comlocate.knosys.

25. V. Ojansivu, J.Heikklä (2008) A. Elmoataz et al. (Eds.): ICISP 2008, LNCS 5099. Springer, Berlin Heidelberg: Blur insensitive texture classification using local phase quantization, 236-243, 2008.
26. Timo Ahonen ; Esa Rahtu ; Ville Ojansivu ; Janne Heikkila. Recognition of blurred faces using Local Phase Quantization. 2008 19th International Conference on Pattern Recognition, 8-11 Dec. 2008. doi: 10.1109/ICPR.2008.4761847.
27. Kechen SONG, Shaopeng HU and Yunhui YAN Automatic recognition of surface defects on hot-rolled steel strip using Scattering Convolution Network. Journal of Computational Information Systems (2014), 10: 7, 3049–3055.
28. Bouhouche Salah, Ziani Slimane, Mentouri Zoheir, Bast Jurgen. Uncertainty estimation of mechanical testing properties using sensitivity analysis and stochastic modeling. Measurement 62 (2015)140-154. https://doi.org/10.1016/j.measurement.2014.10.036.
29. M. W. Ashour, F. Khalid, A. Abdul Halin, L. N. Abdullah and S.H. Darwish Surface defects classification of hot-rolled steel strips using multi-directional shearlet features. Arabian Journal for Science and Engineering. Springer (2018), https://doi.org/10.1007/s13369-018-3329-5.
30. Li Yi, Guangyao Li, and Mingming Jiang An end-to-end steel strip surface defects recognition system based on Convolutional Neural Networks. Steel research int. 87, (2016), N°. 9999. DOI: 10.1002/srin.201600068, available at : www.steel-research.de.
31. Kechen Song and Yunhui Yan A noise robust method based on completed local binary patterns for hot-rolled steel strip surface defects. Applied Surface Science 285P (2013), 858-864, available at : www.elsevier.com/locate/apsusc.